





Insight into Viral Hijacking of CRL4 Ubiquitin Ligase through Structural Analysis of the pUL145-DDB1 Complex

Elizaveta T. Wick,^{a,c} Colton J. Treadway,^{a,c} Zhijun Li,^{b,c} Nathan I. Nicely,^a Zhizhong Ren,^{b,c} Albert S. Baldwin,^c Yue Xiong,^{b,c*}
 Joseph S. Harrison,^d  Nicholas G. Brown^{a,c}

^aDepartment of Pharmacology, University of North Carolina, Chapel Hill, North Carolina, USA

^bDepartment of Biochemistry and Biophysics, University of North Carolina, Chapel Hill, North Carolina, USA

^cLineberger Comprehensive Cancer Center, University of North Carolina at Chapel Hill, Chapel Hill, North Carolina, USA

^dDepartment of Chemistry, University of the Pacific, Stockton, California, USA

ABSTRACT Viruses evolve mechanisms to exploit cellular pathways that increase viral fitness, e.g., enhance viral replication or evade the host cell immune response. The ubiquitin-proteasome system, a fundamental pathway-regulating protein fate in eukaryotes, is hijacked by all seven classes of viruses. Members of the Cullin-RING family of ubiquitin (Ub) ligases are frequently co-opted by divergent viruses because they can target a broad array of substrates by forming multisubunit assemblies comprised of a variety of adapters and substrate receptors. For example, the linker subunit DDB1 in the cullin 4-RING (CRL4)-DDB1 Ub ligase (CRL4^{DDB1}) interacts with an H-box motif found in several unrelated viral proteins, including the V protein of simian virus 5 (SV5-V), the HBx protein of hepatitis B virus (HBV), and the recently identified pUL145 protein of human cytomegalovirus (HCMV). In HCMV-infected cells, pUL145 repurposes CRL4^{DDB1} to target STAT2, a protein vital to the antiviral immune response. However, the details of how these divergent viral sequences hijack DDB1 is not well understood. Here, we use a combination of binding assays, X-ray crystallography, alanine scanning, cell-based assays, and computational analysis to reveal that viral H-box motifs appear to bind to DDB1 with a higher affinity than the H-box motifs from host proteins DCAF1 and DDB2. This analysis reveals that viruses maintain native hot-spot residues in the H-box motif of host DCAFs and also acquire favorable interactions at neighboring residues within the H-box. Overall, these studies reveal how viruses evolve strategies to produce high-affinity binding and quality interactions with DDB1 to repurpose its Ub ligase machinery.

IMPORTANCE Many different viruses modulate the protein machinery required for ubiquitination to enhance viral fitness. Specifically, several viruses hijack the cullin-RING ligase CRL4^{DDB1} to degrade host resistance factors. Human cytomegalovirus (HCMV) encodes pUL145 that redirects CRL4^{DDB1} to evade the immune system through the targeted degradation of the antiviral immune response protein STAT2. However, it is unclear why several viruses bind specific surfaces on ubiquitin ligases to repurpose their activity. We demonstrate that viruses have optimized H-box motifs that bind DDB1 with higher affinity than the H-box of native binders. For viral H-boxes, native interactions are maintained, but additional interactions that are absent in host cell H-boxes are formed, indicating that rewiring CRL4^{DDB1} creates a selective advantage for the virus. The DDB1-pUL145 peptide structure reveals that water-mediated interactions are critical to the higher affinity. Together, our data present an interesting example of how viral evolution can exploit a weakness in the ubiquitination machinery.

KEYWORDS cullin-RING, human cytomegalovirus, innate immunity, ubiquitin ligase, viral hijacking

Editor Lori Frappier, University of Toronto

Copyright © 2022 American Society for Microbiology. All Rights Reserved.

Address correspondence to Joseph S. Harrison, jharrison@pacific.edu, or Nicholas G. Brown, nbrown1@med.unc.edu.

*Present address: Yue Xiong, Cullgen Inc., San Diego, California, USA.

The authors declare a conflict of interest. Y.X. is an inventor named on patent applications filed by UNC. The Xiong laboratory has received research funds from Cullgen, Inc. Y.X. is an equity shareholder in and employee of Cullgen, Inc. All other authors declare no competing interest.

Received 27 May 2022

Accepted 21 July 2022

Published 8 August 2022

Viruses evolve species-specific interactions with host factors that promote viral replication (1). The host pathways that viruses modulate can vary dramatically for different viruses depending on the cell and host range (2). However, many different viruses have evolved a common mechanism to hijack the ubiquitin (Ub) pathway (3, 4). Ub is targeted to proteins through a trienzyme E1-E2-E3 cascade and is removed by a class of proteases called deubiquitinases (DUBs) (5). Ub is also able to form polyubiquitin chains that control the different outcomes of ubiquitination (e.g., K63 polyubiquitination-dependent targeting to the endosome) (6–11). The most well studied outcome of polyubiquitination is to promote proteasomal degradation of the target protein, controlling cell cycle control, DNA repair, gene expression, and immune signaling (11). Viruses have evolved many different strategies to disrupt normal cellular ubiquitination pathways, such as encoding their own DUBs, incorporating motifs to induce ubiquitination, and altering substrate ubiquitination (3, 4, 12–17). Together, these changes are required for several aspects of the viral life cycle, such as gene transcription, downregulation of host immune signaling, and viral maturation and budding.

The recruitment of substrates to an E3 Ub ligase and subsequent polyubiquitination is often dictated by hierarchical assemblies that contain multiple subunits. The cullin-RING ligase (CRL) family of Ub ligases is composed of cullin (CUL) scaffolds (cullin 1–5, 7, and 9) and RING-containing proteins (ROC/RBX 1–2) (18). CRLs are hijacked by several viruses to alter the cell cycle or the immune response, especially CUL4-ROC1 (CRL4) (13, 19, 20). To recruit substrates, CUL4 binds to the DNA-damage-binding protein 1 (DDB1), which in turn recruits multiple substrate receptors that give CRL4 its substrate specificity by forming ~90 different CRL4 complexes (21–25). Several viruses tap into these assembly mechanisms to recruit new substrates to CRL4 for polyubiquitination and degradation (26).

One family of substrate receptors that binds to DDB1 are DCAF (DDB1 and CUL4-associated factors) proteins (27). Several DCAF family members bind to DDB1 through a degenerate α -helical H-box motif (Fig. 1A) (28–30). In addition, several unrelated viral proteins have also evolved distinct H-box motifs to rewire CRL4 activity, e.g., hepatitis B viral regulator protein HBx and simian virus 5 V (SV5-V) (20, 22, 26, 31–34). Recently, a new H-box-containing protein, pUL145, was identified in human cytomegalovirus (HCMV) that hijacks CRL4^{DDB1} to disrupt the innate immune response by ubiquitinating the signal transducer and activator of transcription 2 (STAT2) (35). Furthermore, helicase-like transcription factor (HLTF) and p53-binding protein 1 (53BP1) have also been identified as host cell targets (36). Interestingly, the sequence of this new H-box seems relatively different compared to the other H-box family members with multiple charged residues at its C terminus (Fig. 1B) (34, 37).

Despite the large number of abundant proteins that bind to the same H-box binding groove on DDB1, H-box motif sequences vary widely (Fig. 1B) (31, 37). Therefore, it remains unclear what H-box residues are strictly required for the binding and specific interactions with DDB1. Furthermore, it is poorly understood how viral H-box-containing proteins, including pUL145, can bind and repurpose the CRL4^{DDB1} complex when there are dozens of abundant cellular DCAFs. Here, we performed alanine-scanning mutagenesis, crystallography, computational analysis (sequence conservation and molecular modeling), and cell-based binding and protein degradation assays to understand what residues on the H-box and DDB1 determine the binding affinity of the DDB1-H-box interaction. Our results reveal that viral H-boxes share conserved hot-spot residues with the human H-boxes but have more optimized residues to bind DDB1 at the variable positions of the sequence, including the C terminus of the motif. For example, an H-box peptide derived from the pUL145 sequence had the highest binding affinity (24 nM), partly because of a unique water-mediated interaction at the C terminus of the H-box. Furthermore, we show that mutations to the pUL145 H-box or the H-box binding groove of DDB1 are sufficient to disrupt STAT2 degradation, highlighting the importance of the H-box-DDB1 interaction to CRL4 hijacking. Overall, these studies provide valuable information about the specificity

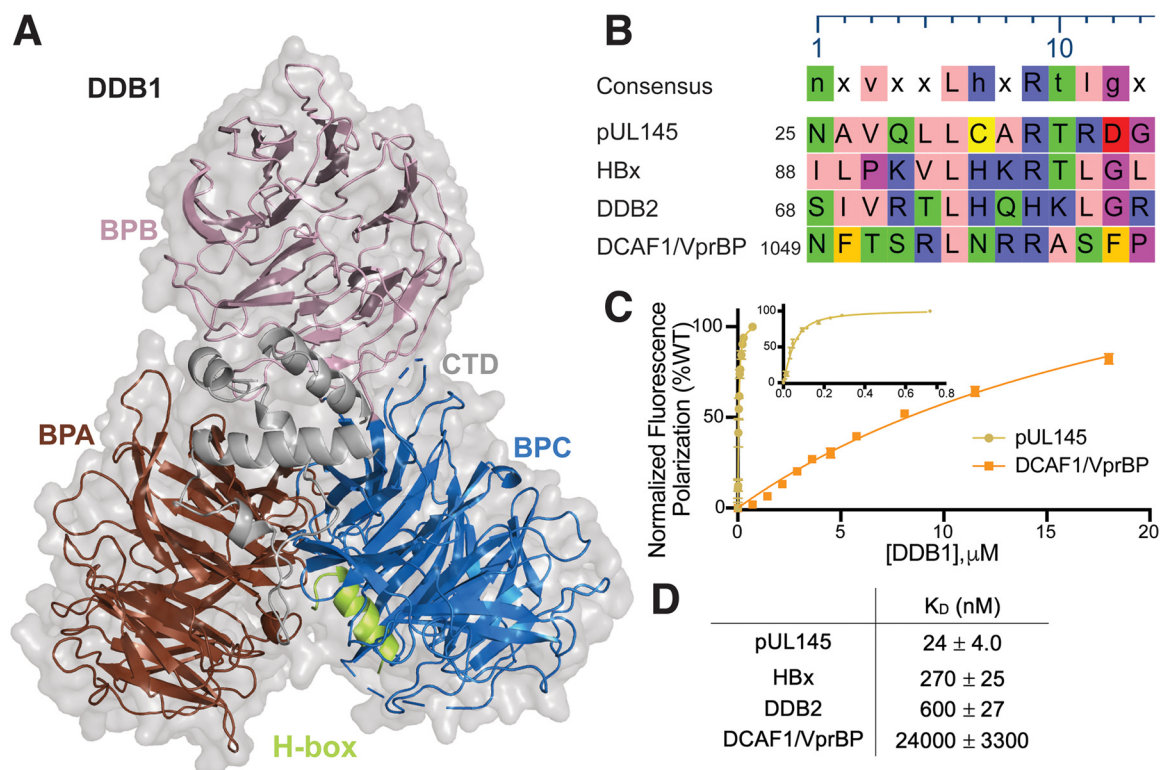


FIG 1 Viral H-boxes bind tighter than the human H-boxes used in this study to DDB1. (A) Structure of DDB1 bound to the H-box peptide (green) from HBx (Protein Data Bank code 3I7H) (31). DDB1 consists of three β -propellers (multicolored), but the H-box peptide predominantly interacts with β -propeller C (BPC). (B) The H-box consensus sequence was created using MegAlign from Lasergene. The amino acids are highlighted according to their physicochemical properties. (C) Representative fluorescence polarization (FP) data indicating the binding of H-box peptides from pUL145 or DCAF1 to DDB1. The experiments were performed in at least triplicate and normalized to wild type (WT) as 100%. (D) Table of the affinities (K_D) and standard deviations for the tested H-boxes against DDB1 based on FP data in panel C. BPA, β -propeller A; BPB, β -propeller B; BPC, β -propeller C; CTD, C-terminal domain.

of the H-box motif and how viral evolution can optimize binding interfaces in unexpected ways to alter cell signaling.

RESULTS

DDB1 binds to different H-boxes with a wide range of affinities. To understand how viral proteins can rewire CRL4^{DDB1}, we examined the binding constants of H-box peptides from two host proteins, DCAF1/VprBP and DDB2, and two viral proteins, HBx and pUL145 (20, 26, 28–31, 33, 35). Fluorescence polarization (FP) assays were used to determine the dissociation constants for DDB1 and fluorescently labeled H-box peptides. Interestingly, both peptides derived from viral proteins bound tighter than the host proteins to DDB1 (Fig. 1C and D). In particular, the pUL145 H-box was a significantly tighter binder and required the fitting of the binding constants using a quadratic function that accounts for peptide depletion. The pUL145-derived and HBx-derived peptides bound to DDB1 with equilibrium dissociation constant (K_D) values of 24 ± 4 nM and 270 ± 25 nM, respectively. In contrast, the DCAF1- and DDB2-derived peptides displayed $\sim 1,000$ - and ~ 25 -fold weaker affinity compared to the pUL145 H-box, respectively, and ~ 88 - and ~ 2 -fold compared to the HBx H-box, respectively. These data suggest that the high affinity of viral H-box peptides to DDB1, compared to host H-box motifs, helps viruses rewire the substrate targeting of CRL4^{DDB1}.

Identification of the pUL145 H-box residues responsible for the tight binding affinity for DDB1. To better understand the sequence determinants that give the pUL145 H-box a higher affinity for DDB1, we performed alanine scanning of the H-box peptide. In this set of peptides, each position of the H-box motif was changed to alanine, except for A26 at position 2 (Pos2) and A32 at Pos8, where alanine was already

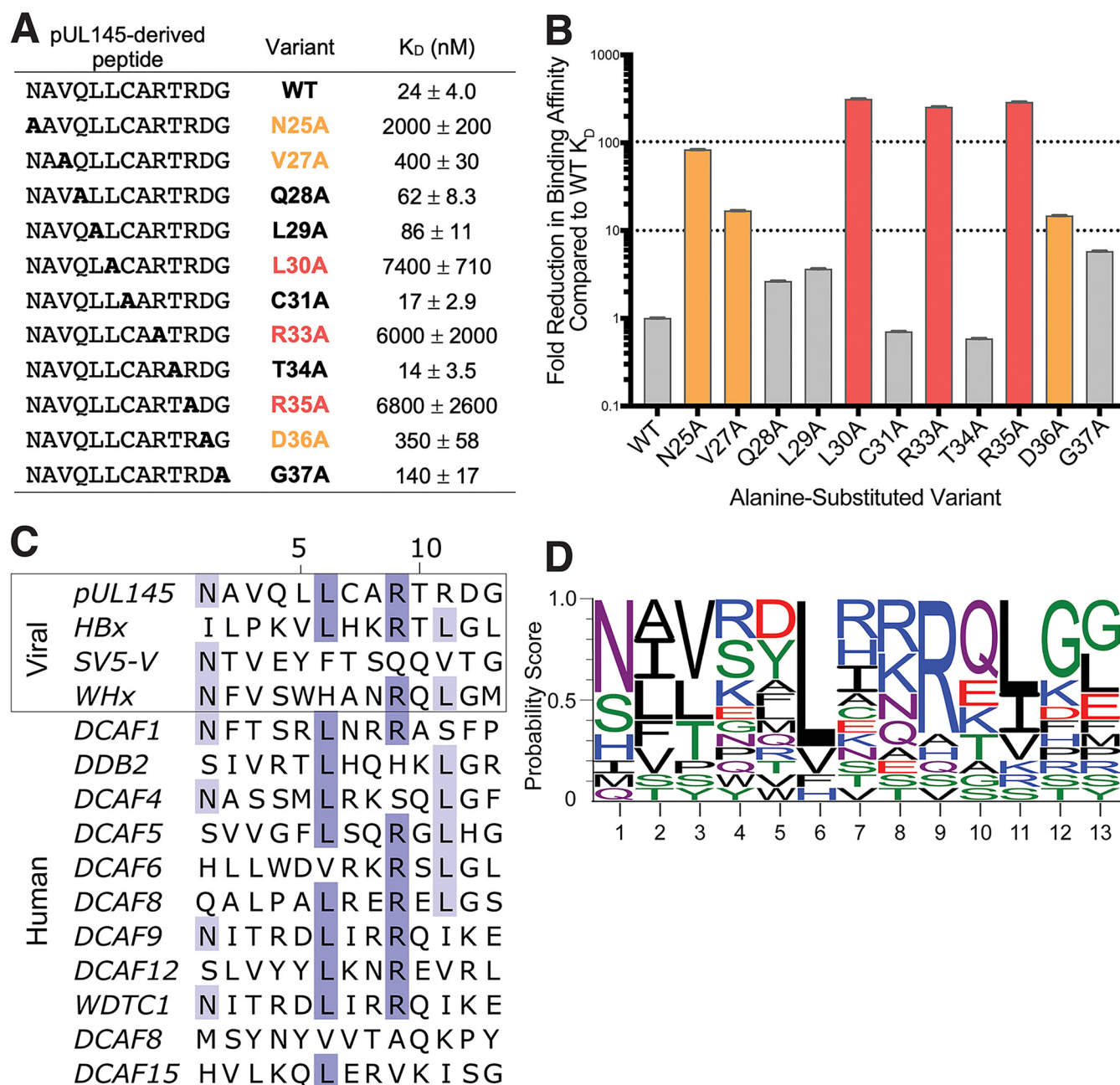


FIG 2 Sequence requirements for H-box binding affinity for DDB1. (A) Table of K_D values and standard deviations for a panel of pUL145 H-box peptides in which the indicated residues were substituted to Ala. The colors of the labels correspond to the magnitude of the fold reduction in binding affinity when the native residue is replaced with Ala (red indicates >100-fold, orange indicates >10-fold, and gray indicates <10-fold). (B) Bar graph of the data from panel A comparing the binding affinities for the alanine-substituted pUL145 peptides. The y axis represents the reduction (fold change) of binding compared to the wild-type peptide. The colors are the same as in panel A. The error bars represent standard deviations. (C) Sequence alignment of known H-boxes that bind to DDB1 with conserved residues shaded. (D) WebLogos of the H-box sequence based on the sequence alignment from panel C colored by their physicochemical properties.

present. These fluorescently labeled peptides were then tested in our FP assay against DDB1 to determine their binding affinity (Fig. 2A). The side chains of six residues displayed more than a >10-fold decrease in binding when changed to Ala: N25(Pos1), V27(Pos3), L30(Pos6), R33(Pos9), R35(Pos11), and D36(Pos12) (Fig. 2B). Of these residues, three alanine-substituted variants that resulted in the largest defect in binding were L30(Pos6), R33(Pos9), and R35(Pos11), all of which resulted a greater than 200-fold decrease in binding affinity.

To put these results in context with other known H-boxes, we structurally aligned the

crystallized DDB1-H-box complexes and analyzed the sequences (Fig. 2C). Expectedly, there is a strong conservation of Leu at Pos6 and Arg at Pos9, which is important for pUL145 binding to DDB1. Surprisingly, the conservation of Leu at Pos11 and Gly at Pos12 is not maintained in pUL145, which has an Arg at Pos11 and Asp at Pos12. The other residues of the H-box motif displayed far more variability. However, all six of the binding residues we identified have some degree of sequence identity based on the BLOSUM62 substitution matrix (Fig. 2D). Together, these sequence alignments and alanine-scanning results are highly correlated, revealing that the binding epitope consists of the six residues, but L30 (Pos6), R33(Pos9), and R35(Pos11) are the hot spots that displayed >200-fold decreases in binding when substituted for Ala.

Crystal structure of DDB1 bound to the pUL145 H-box peptide. To further characterize how the pUL145 H-box has evolved to bind DDB1, we determined the structure of DDB1 bound to a pUL145 peptide containing residues N25 through G37 to 2.9 Å resolution (Fig. 3A; Table 1). The DDB1-pUL145 H-box structure contained one complex per asymmetric unit. Overall, the structure of the pUL145 peptide bound to DDB1 was similar to other H-box-DDB1 structures with a root mean square deviation (RMSD) of 0.34 to 0.94 Å for the entire structure of the complex and 0.16 to 0.43 Å for the H-box peptide (Fig. 3B) (28, 30, 31). The α -helical H-box was positioned in a binding groove that is enclosed by the BPA-BPC double propeller fold with most of its interactions occurring with BPC. The pUL145 H-box-DDB1 complex revealed several conserved interactions. First, the N-terminal residue, N25(Pos1), interacts with a loop of DDB1 (residues 836 to 841). Second, V27(Pos3) forms hydrophobic interactions with L814 and V836 of DDB1. Third, the vital L30(Pos6) forms additional hydrophobic interactions with L912 and L926. Last, R33(Pos9) sticks into a pocket that is formed between multiple loops of the β -propeller and forms a hydrogen bond with Y913 (Fig. 3C to F). All of these interactions are largely conserved among the known structures.

However, an area that is clearly divergent is the C terminus of pUL145. In previous structures, residues at Pos11 and Pos12 of the H-box are hydrophobic, often Leu, followed by a glycine or positively charged residues, respectively. The conserved Leu at Pos11 interacts with a hydrophobic patch comprised of L328, P358, A381, and F382. However, for pUL145, Pos11 is R35 instead of a conserved Leu, and Pos12 is D36. Unexpectedly, the R35A substituted variant of the pUL145 H-box resulted in an \sim 290-fold decrease in binding affinity compared to wild type. Similar to a conserved Leu residue, composition of R35 allows it to fulfill the extensive interactions with the hydrophobic patch of L328, P358, A381, and F382 (Fig. 3G). Additional interactions at the pUL145 C terminus include N1005 hydrogen bonding to the backbone of T34(Pos10) and R327 interacting with the backbone of the H-box C terminus (Fig. 3H and I).

Despite the importance of the pUL145 residues D36(Pos11) and G37(Pos12) observed in the binding assays (Fig. 2A and B), when examining the crystal structure, there were surprisingly few direct contacts between these residues and DDB1. D36(Pos12) is in a hydrophobic pocket between F972, F1003, and V1033 in which only the C- β of D36 (Pos12) is within 4.0 Å of V1033. The carboxylic acid side chains would also yield unfavorable unsatisfied hydrogen bond sites. Upon closer examination of the electron density, we observed density for a water molecule (B factor of 5) that is coordinated between K60 of DDB1 and D36(Pos12) of pUL145. This coordinated water likely enhances the binding affinity of the pUL145 H-box for DDB1 because the substitution of this side chain for Ala resulted in a 14-fold decrease in K_D (Fig. 3J).

Determination of the hot-spot residues of DDB1 responsible for pUL145 H-box recognition through alanine-scanning mutagenesis. Based on the structure alone, it is unclear why the pUL145 H-box has a higher affinity to DDB1 than other H-boxes. The H-box binding groove in DDB1 recognizes many helical peptide sequences with divergent sequences. To further understand the binding determinants for DDB1, we purified a set of 21 DDB1 variants in which the residues within 4 Å of the H-box motif were substituted to Ala and tested for binding to pUL145 H-box using FP. Several variants exhibited a dramatically reduced affinity for the pUL145 H-box peptide, ranging

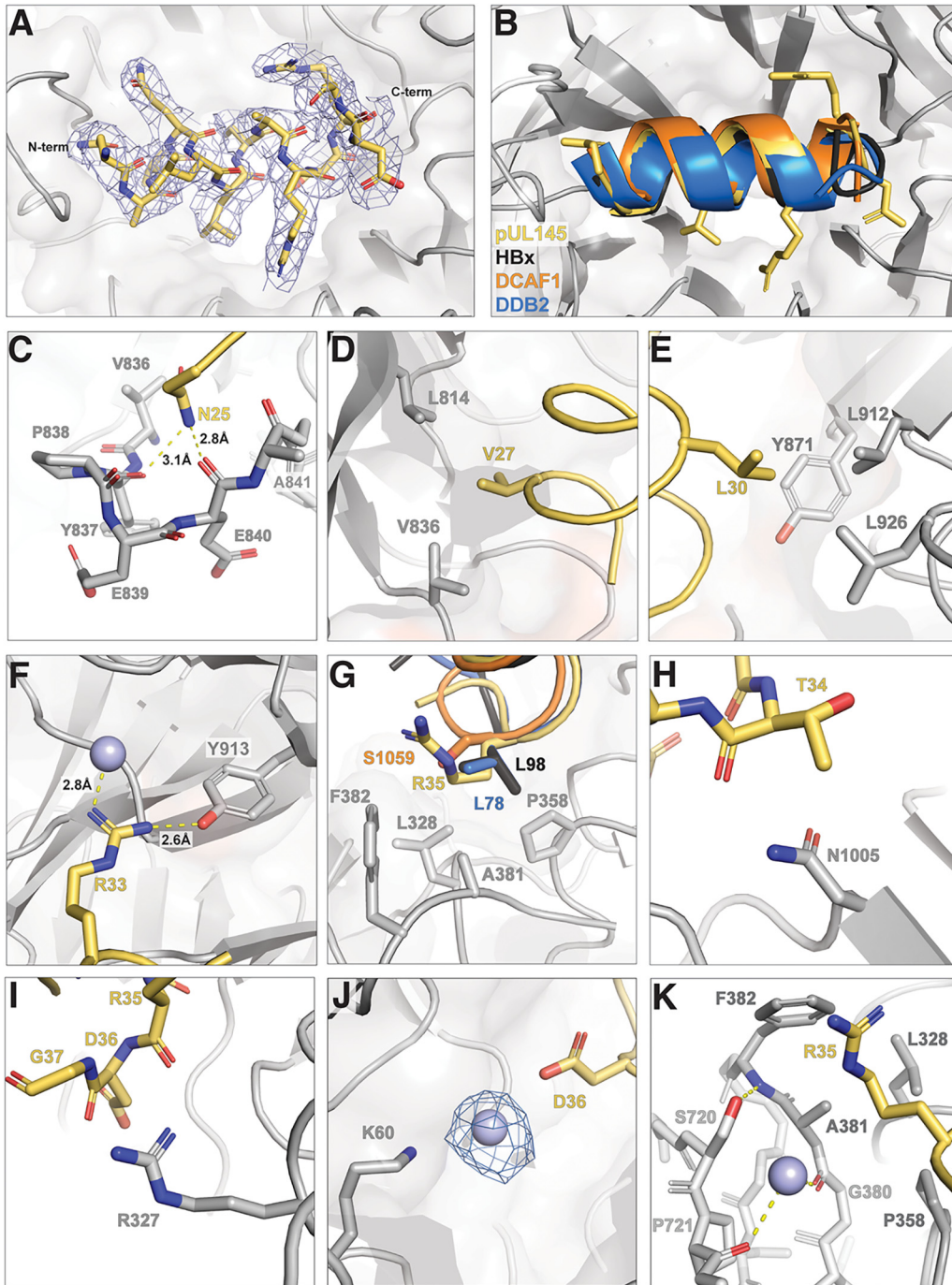


FIG 3 Crystal structures of the H-box peptide derived from pUL145 bound to DDB1. (A) Close-up view of the pUL145 H-box peptide (yellow) in complex with DDB1 (gray). The $2F_o - F_c$ electron density map is contoured at 1σ . (B) Superposition of the H-box peptides of HBx (black, PDB ID 3I7H), DDB2 (blue, PDB ID 3I7L), DCAF1 (orange, PDB ID 5JK7), and pUL145 (yellow, PDB ID 7UKN) bound to DDB1 (30, 31). (C to K) Close-up views of the key interactions between pUL145 (yellow), DDB1 (gray), and water (gray sphere) based on the binding affinities of the alanine-substituted pUL145 H-box peptides. The $2F_o - F_c$ electron density map is contoured at 1σ .

from 24 to 2,300 nM (Table 2; Fig. 4A). Together, these values allowed us to map the hot-spot residues of DDB1 binding to the pUL145 H-box.

Residues in DDB1 that contribute to H-box recognition are defined as having a >10-fold decrease in binding affinity based on the K_D values determined by FP. Therefore, 12 residues, R327A, L328A, V360A, S720A, Y812A, L814A, V836A, Y871A, L912A, L926A, F1003A, and

TABLE 1 Crystal and X-ray diffraction data of DDB1-pUL145 H-box peptide

Parameter	Value
Wavelength	1 Å
Resolution range ^a	46.21–2.90
Space group	P 2 ₁ 2 ₁ 2 ₁
Unit cell	
<i>a</i> , <i>b</i> , <i>c</i> (Å)	63.5, 134.7, 183.0
α , β , γ (°)	90, 90, 90
Total reflections ^b	36,461 (1,775)
Unique reflections	34,718 (2,877)
Multiplicity	6.3 (6.6)
Completeness (%)	97.37 (82.67)
Mean <i>I</i> / σ (<i>I</i>)	12.7 (1.37)
Wilson B factor	50.78
<i>R</i> _{merge}	0.132 (1.793)
<i>R</i> _{meas}	0.180 (2.202)
<i>R</i> _{pim}	0.070 (0.840)
CC1/2	0.992 (0.488)
CC*	0.998 (0.810)
Reflections used in refinement	34,713 (2,877)
Reflections used for <i>R</i> _{free}	1,972 (164)
<i>R</i> _{work}	0.194 (0.270)
<i>R</i> _{free}	0.261 (0.365)
No. of nonhydrogen atoms	8,415
Macromolecules	8,401
Solvent	14
Protein residues	1,072
RMS (bonds)	0.009
RMS (angles)	1.23
Ramachandran favored (%)	89.48
Ramachandran allowed (%)	9.18
Ramachandran outliers (%)	1.34
Rotamer outliers (%)	0.21
Clashscore	10.94
Avg B-factor	58.62
Macromolecules	58.68
Solvent	23.68
No. of TLS groups	5

^aThe resolution range for collected data is 46.21–2.87 Å; the resolution range for the refined structure is 46.21–2.90 Å. Resolution was truncated to improve the completeness.

^bThe numbers in parentheses refer to the relevant outer resolution shell.

N1005A, are a part of the H-box binding groove, which can be loosely divided into three segments (Fig. 4A and B). First, the N terminus of the helical peptide is stabilized by hydrophobic interactions between L814 and V836 of DDB1 and V27(Pos3) of pUL145 (Fig. 3C and D and 4C). Notably, the V836A substitution on DDB1 had the largest change in binding affinity, ~80-fold, denoting the significance of binding to the N terminus of the H-box (Fig. 4A). Y812 and Y871 of DDB1 also form hydrogen bonds with the N-terminal residues of the pUL145 H-box. These interactions are relatively conserved among H-boxes despite the sequence differences due to the chemical and size similarities between the amino acid side chains found at this position (Fig. 2D).

The second segment contains the two most conserved residues L30(Pos6) and R33(Pos9) of the H-box (Fig. 3E and F and 4). It is formed by several hydrophobic residues, including Y871, L912, L926, and W953. Y871 and L912 of DDB1 form van der Waals interactions with L30(Pos6). However, L926 is too far away to contact pUL145 directly but may instead stabilize L912 and the rest of the hydrophobic surfaces. Furthermore,

TABLE 2 Dissociation constants of DDB1 WT and alanine-substituted variants^a

DDB1 variants	K_D (nM)
WT	24 ± 4.0
R327A	740 ± 140
L328A	300 ± 19
V360A	330 ± 23
F382A	72 ± 13
S720A	780 ± 150
R722A	91 ± 12
K723A	150 ± 29
E787A	180 ± 37
Y812A	680 ± 130
L814A	450 ± 45
V836A	2,300 ± 290
Y871A	750 ± 100
M910A	62 ± 8.8
L912A	310 ± 64
L926A	620 ± 83
W953A	70 ± 10
S955A	59 ± 5.6
N970A	77 ± 24
F1003A	760 ± 130
N1005A	720 ± 43
V1033A	59 ± 7.9

^aWT, wild-type.

we observe the backbone of L926 coordinating a water molecule that hydrogen bonds to R33(Pos9). Also, the aliphatic portion of the R33(Pos9) side chain is coordinated by F1003. This portion of the interaction represents the binding pocket of the most conserved residues in our alignment and also results in the greatest defects when mutated to alanine, suggesting that this region is the dominant hot spot used by both human and viral H-boxes.

Last, the C terminus of the H-box recognizes five residues in DDB1: R327, L328, V360, S720 and N1005 (Fig. 3G and 4C). R327 makes interactions with the backbone of the H-box (Fig. 3I). N1005 hydrogen bonds with the backbone of the T34(Pos10) carbonyl (Fig. 3H). R35 (Pos11), which is normally Leu in other H-boxes, binds in this region as well. Interestingly, the R35 (Pos11) interaction with F382 did not significantly contribute to binding, but S720 scored as a part of the binding groove. Based on the structure, S720 is involved in a complex electrostatic network. It facilitates a hydrogen bond with the backbone of F382, which stabilizes the hydrophobic patch consisting of L328, P358, A381, and F382 residues. Additionally, the neighboring G380 and P721 coordinate a water molecule that participates in electrostatic interactions with S720 and R35 on pUL145 (Fig. 3K).

To evaluate the significance of the identified DDB1 and pUL145 residues in STAT2 degradation, we performed a series of cell-based experiments. First, HEK293T cells were transfected with both FLAG-tagged DDB1 and MYC-tagged pUL145. As expected, pUL145 coimmunoprecipitated with FLAG-tagged DDB1 (Fig. 4D), and DDB1 coimmunoprecipitated with MYC-tagged pUL145 (Fig. 4E). However, when mutations were introduced into either DDB1 (V836A) or pUL145 (L30A and D36A), these interactions were largely reduced (Fig. 4D and E). We also monitored the pUL145-mediated degradation of STAT2 during these experiments. Consistently, expression of pUL145 correlated with lower levels of STAT2 (Fig. 4D to F). Even though the cells contained endogenous DDB1, resulting in some variability in pUL145-mediated STAT2 degradation, overexpression of the DDB1 V836A protein significantly rescued the amount of STAT2 present. Furthermore, by introducing L30A and D36A mutants of pUL145, STAT2 protein levels returned to near native levels (Fig. 4D to F). Together, these results were highly similar to our *in vitro* binding data and indicate the importance of the intact H-box for pUL145-dependent STAT2 degradation.

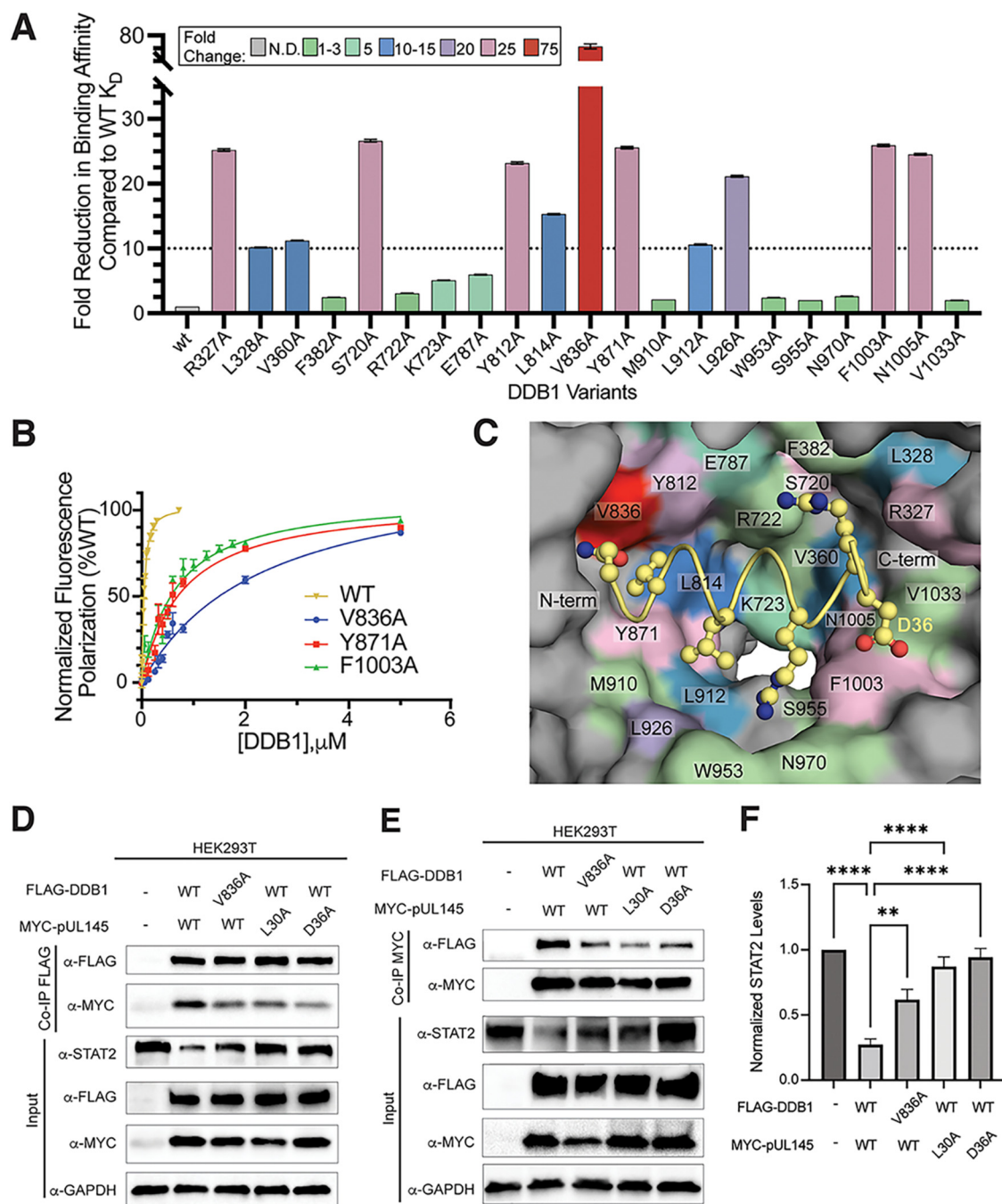


FIG 4 Functional epitope of DDB1 for binding H-box sequences. (A) Bar graph of the data shown in Table 2 comparing the binding affinities for the alanine-substituted DDB1 variants. The y-axis represents the reduction (fold change) in binding compared to wild-type DDB1. The colors of the bars correspond to the extent of the fold change in binding affinity because of the alanine substitution. The error bars represent the standard deviations. (B) Representative fits of FP data to determine the binding affinity of DDB1 wild-type and the alanine-substituted variants. Experiments were performed in at least triplicate and normalized to WT as 100%. (C) Surface view representation of DDB1 bound to pUL145 (atoms shown as spheres). DDB1 residues mutated in this study are colored as a gradient to indicate the increasing reduction in binding affinity compared to wild-type DDB1. (D, E) DDB1 and pUL145 variants reduce the interaction and disturb STAT2 degradation, monitored by coimmunoprecipitation (Co-IP) and Western blotting. HEK293T cells were transiently transfected with FLAG-tagged DDB1 and MYC-tagged pUL145 or GFP as a negative control. Cell extracts were prepared, and the pUL145-DDB1 complex was coimmunoprecipitated using an antibody to either the FLAG (D) or MYC (E) tag ($n \geq 3$). The STAT2 levels were also monitored by immunoblotting the inputs of the co-IP ($n = 7$). (F) STAT2 levels in HEK293T cells transfected with DDB1 and pUL145 wild-type and variants from panels D and E. STAT2 levels were calculated as ratios compared to the loading control glyceraldehyde-3-phosphate dehydrogenase (GAPDH) and normalized to the levels of STAT2 in control cells. The error bars represent standard error. Statistical significance was assessed by one-way analysis of variance (ANOVA). **, $P \leq 0.01$; ****, $P \leq 0.0001$ ($n = 7$ biological replicates). N.D., not determined.

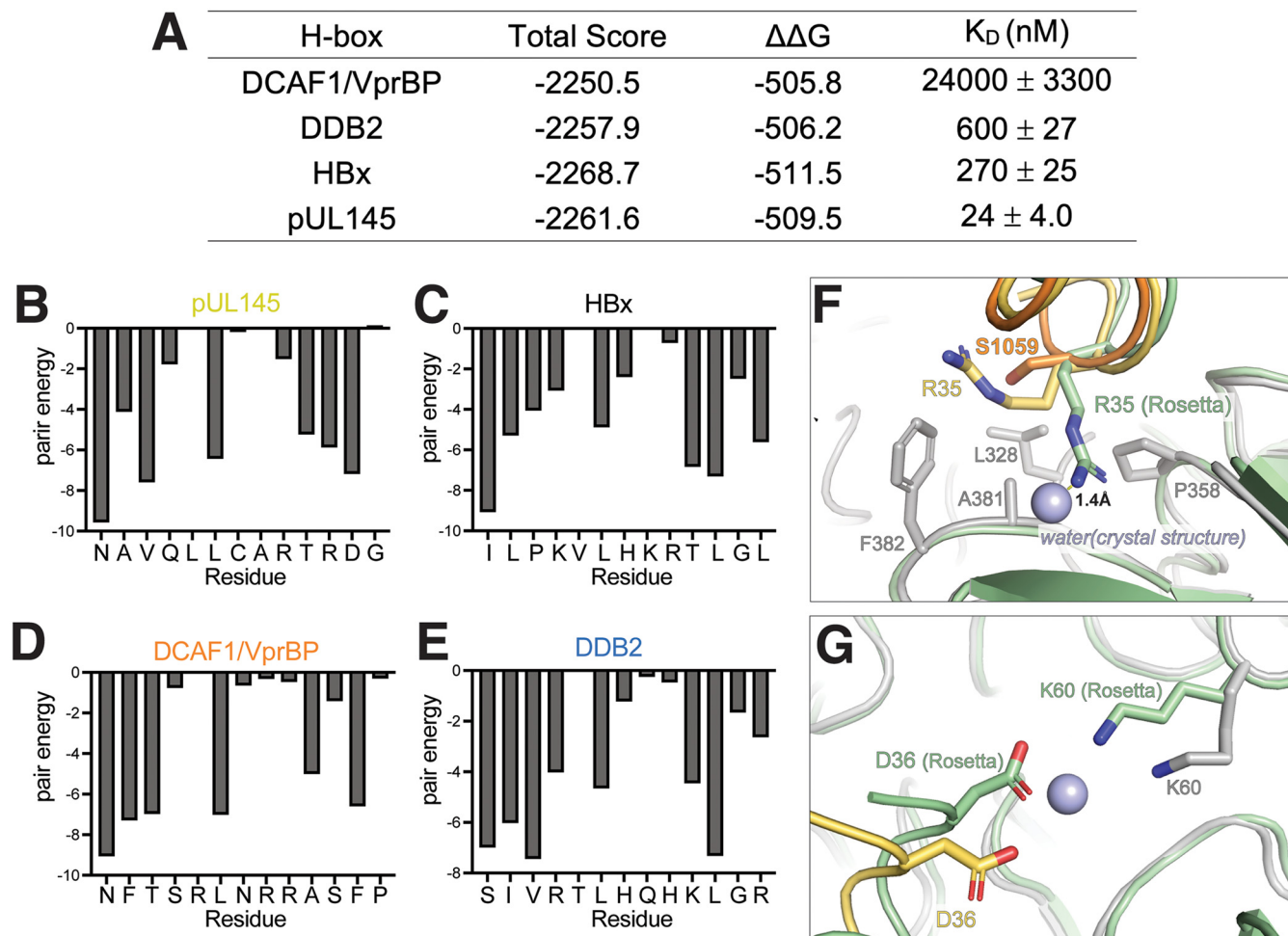


FIG 5 Viral sequences tend to form additional interactions at the C terminus of the H-box sequence to facilitate tighter binding. (A) Table of H-box-DDB1 Rosetta energies of the lowest scoring structure. The total energy is the overall Rosetta energy of the structure, and $\Delta\Delta G$ represents the computational binding energy. It is calculated by subtracting the Rosetta energy for the complex by the energy of the isolated DDB1 and H-box structures. The affinities (K_D) were determined experimentally from Fig. 1 (B to E) Rosetta pair energies of the H-box peptide residue interactions with DDB1 using pUL145 (B), HBx (C), DCAF1 (D), and DDB2 (E). (F, G) Structural comparison of the Rosetta models (green) and crystal structure of DDB1 (gray) bound to the pUL145 (yellow) or DCAF1 (orange) H-box peptide demonstrate that Rosetta formed alternative favorable interactions for R35 and D36 where bridging water molecules were identified in the crystal structure.

Computational analysis of H-box binding to DDB1. Although we have analyzed pUL145 H-box binding to DDB1, it remained unclear why the pUL145 H-box has such a high affinity compared to the DCAF1 H-box, which displayed markedly poor affinity for DDB1. Thus, we turned to computational methods in Rosetta to help dissect the residue contributions to binding by creating a model with truncated DDB1-pUL145. We installed the H-box sequences from DCAF1, DDB2, or HBx using fixed backbone design (fixbb) and then ran 100 all-atom refinement simulations (relax) on each H-box model. The total Rosetta-energy (REU) score and REU- $\Delta\Delta G$ for binding matched the trends we observed for the peptide affinities: DCAF1 > DDB2 > HBx/pUL145 (Fig. 5A). Next, we analyzed the residue-residue REU score for the DDB1-H-box interactions for each H-box residue from the lowest scoring model. Overall, the results match the biochemical data well, with Pos1, Pos3, Pos6, and Pos11 containing important binding residues (Fig. 5B to E). Rosetta also indicates that Pos2 and Pos10 are important for binding. In the pUL145 H-box, Pos2 is already Ala and was not tested but is buried at the interface. On the other hand, T34A (Pos10) did not result in a binding defect, but Rosetta also scores the Ala in the DCAF1 H-box sequence favorably. Together, this suggests that Rosetta-based calculations could provide insight into the recognition of the DCAF1 H-box by DDB1.

Rosetta indeed provided an explanation for how viral H-boxes evolved to hijack

DDB1. First, the weaker binding H-box peptide of DCAF1 makes poorer interactions than the other tested H-boxes. DCAF1 has a Ser at Pos11 that is ~ 5 REU less favorable than those with Leu or Arg at that position (Fig. 5F). DCAF1 also has a Ser at Pos4 that contributes less to binding than the other H-boxes. Examination of the DCAF1-DDB1 structure reveals that these interactions are not very favorable. Second, while the overall binding energies from the N-terminal portion of all of the peptides are similar, the C terminus of the viral H-boxes appear to be better at binding than the human sequences (Fig. 5B to E). When looking at the last three residues of the H-box motif, both the human sequences have only one residue below -5 REU, while both of the viral sequences have two: HBx contains L98(Pos11) and L100(Pos13), and pUL145 has R35(Pos11) and D36(Pos12) (Fig. 5B to E). This analysis reveals how viral H-boxes optimize their sequences to maximize contacts at neighboring sites in the binding groove.

Interestingly, Rosetta scores D36(Pos12) as very favorable, so we looked more closely at the pair score energies and saw that in the model there was a very favorable interaction energy (< -4 REU) between K60 and D36(Pos12). In the modeling, Rosetta predicted an extend K60 rotamer and altered the C terminus of the backbone of the H-box peptide by > 1 Å, so that a strong electrostatic interaction could form between the two residues (Fig. 5G). While the crystal structure does not have this interaction, it instead has a bridging water molecule between K60 and D36(Pos12). This provides a rationale for why Rosetta was unable to discriminate between the binding affinities of the H-boxes from pUL145 and HBx since the default Rosetta scoring does not consider water bridging interactions. Significantly, pUL145 has the only H-box that has a residue capable of making this type of interaction, and we speculate that this interaction network is one of the reasons that the pUL145 H-box has the highest affinity for DDB1 (38). These data are supported by our in-cell experiments showing that the D36A mutation completely disrupts the coimmunoprecipitation of DDB1 and STAT2 degradation. We also noticed that the R35 rotamer for the crystal structure and Rosetta structure differed and that the position of R35 in Rosetta overlapped with a crystallographic water (Fig. 5F). Therefore, Rosetta suggests that there are other favorable conformations for R35 and D36, even if the crystallographic waters are an artifact of using a peptide rather than the full-length pUL145. Overall, this analysis indicates how thermodynamics of binding is a factor in driving viral evolution.

DISCUSSION

Many unrelated viruses have evolved proteins that contain H-box motifs to repurpose CRL4^{DDB1}. For example, HCMV uses a protein pUL145 to rewire CRL4^{DDB1} to downregulate the antiviral immune response by polyubiquitinating STAT2 (35). This function is similar to simian virus 5 protein (SV5) and hinges on the H-box motif binding to DDB1 (35, 39). Interestingly, HCMV has evolved a number of other proteins that can interact with CRL4 and degrade many host factors, such as SLFN11 (40, 41). Many other viruses also exploit CRL4 (42, 43), e.g., hepatitis virus B HBx degrades host resistance factors, such as SMC5/6 (20, 26, 33). The HBx interaction with DDB1 is also required to activate transcription of viral genes, in part through binding to the arginine methyl transferase PRMT1 (20, 33, 44). Therefore, exploiting DDB1 binding recognition appears to be a common strategy that several viruses have evolved to optimize viral fitness and is consistent with the biological data showing how important the viral H-box proteins are for viremia (45, 46). However, there are many CRL4^{DDB1} host cell substrate receptors that share this binding groove, along with other surfaces, on DDB1, making it unclear how a single viral protein reprioritizes substrate ubiquitination (27, 28, 30, 31).

Here, we show that viral H-box sequences maintain or improve on the hot-spot binding residues found in human H-boxes and form new contacts within the H-box binding groove of DDB1. For the H-box peptides tested, these additional surfaces improve the binding affinity of the viral H-boxes for DDB1 compared to human sequences. For example, L30(Pos6) and R33(Pos9) are relatively invariant in both human and viral sequences, and their substitution to alanine reduces binding to DDB1

by ~100-fold. However, the C-terminal residues of viral H-boxes are optimized for improved interactions and tighter affinity than the host cell H-boxes we tested, providing a selective advantage for viral hijacking. Surprisingly, we found that the H-box from human DCAF1 in isolation from the rest of the protein had a very low affinity for the DDB1 receptor, even though DCAF1 is the most abundant H-box-containing substrate receptor (47). While we do not incorporate other interactions between DDB1 and DCAF1 in this study, the viral H-boxes have a thermodynamic advantage over the DCAF1 H-box, allowing many viruses to populate and exploit CRL4^{DDB1} machinery. It will be interesting to explore how this competition for the H-box binding groove on DDB1 is affected by additional DCAF-DDB1 contacts in future work.

To explore how viral H-boxes optimize their sequence to utilize CRL4^{DDB1}, we determined the crystal structure of an H-box from HCMV pUL145 and substituted both the peptide and DDB1 residues for alanine. Interestingly, we revealed multiple solvent-mediated interactions that improve pUL145 H-box binding to DDB1. First, we identified a unique Arg at Pos11 as a hot spot. In addition to the regular hydrophobic interactions commonly found at this position, C-terminal residues participate in electrostatic interactions with a water molecule coordinated by the backbones of P721 and G380 (Fig. 3K). Furthermore, we observe a unique water-coordinated interaction between K60 of DDB1 and D36(Pos12) of the pUL145 H-box (Fig. 3J). Based on the alanine-scanning results, these interactions are highly valuable and stress the importance of structural determination because Rosetta did not predict these solvent-mediated interactions. Together, this pUL145 H-box-DDB1 interaction is a great example for demonstrating how solvent organization is a recurring method to improve the affinity of protein-ligand interactions (38). Interestingly, this might be a feature that aids the plasticity of the DDB1-binding site, which can also bind to other proteins and ligands in different ways.

Overall, the viral H-boxes maintain the conserved hot-spot binding interactions, even if there is amino acid divergence, suggesting that there is selective pressure to maintain these favorable interactions and evolve new ones. The human sequences, however, are typically missing one of the hot spots, e.g., DCAF1 possessing a Ser (Pos11). We speculate that either very high binding affinity for DCAF substrate adaptors to the H-box binding groove of DDB1 is not necessary because additional contacts are formed to other surfaces of DDB1, or creating a tight-binding interaction may even be detrimental for native CRL4 activity given that rapid assembly/disassembly of CRLs may be important for their function. This feature of CRLs likely provides a weakness for viruses to exploit and suggests that viral H-boxes may repurpose the numerous native CRL4^{DDB1} host cell substrate receptors to hijack CRL4^{DDB1} and degrade host restriction factors (26, 40, 48). In a recent analysis of the HCMV interactome, nearly a dozen viral proteins were found to interact with components of the CRL4^{DDB1} ubiquitin ligase alone (40, 49). As many other viral proteins are known to repurpose or dysregulate several different Ub ligases, it will be exciting to uncover the evolution of improved virus-host Ub ligase interactions that improve viral fitness.

MATERIALS AND METHODS

Site-directed mutagenesis. pFastbac-HTB-DDB1 mutants were cloned by site-directed mutagenesis or overlap extension (50).

Protein expression and purification. For crystallography, DDB1 was overexpressed with a TEV-cleavable, N-terminal His tag in SF9 cells and purified by nickel-affinity chromatography. After TEV cleavage, DDB1 was further purified by anion-exchange chromatography and then size-exclusion chromatography into a final buffer of 20 mM Tris (pH 8.0), 200 mM NaCl, 5 mM dithiothreitol (DTT).

For fluorescent polarization assays, wild-type and alanine-substituted variants of DDB1 were overexpressed in Tni insect cells (Expression Systems). The proteins were purified by nickel-affinity, anion-exchange, and size-exclusion chromatography into 20 mM HEPES (pH 8), 200 mM NaCl, 1 mM DTT. All proteins were flash frozen and stored at -80°C .

Fluorescent polarization. A solution of the 6-carboxytetramethylrhodamine (TAMRA)-tagged peptides (final concentration, 50 nM) was added to solutions of DDB1 variants in assay buffer containing 20 mM HEPES (pH 8), 200 mM NaCl, 0.25 mg/mL bovine serum albumin (BSA), and 0.005% Tween 20. The peptide and DDB1 mixture was incubated on ice for 20 min and then pipetted to a 96-well plate at room temperature. The fluorescence polarization was then measured on the Tecan Spark Cyto with an excitation wavelength of 547 nm (bandwidth, 10 nm) and an emission wavelength of 579 nm (bandwidth, 10 nm).

The data were analyzed in GraphPad Prism using a quadratic equation ($Y = \frac{V_o \left([E_t + X + K_d] - \sqrt{[E_t + X + K_d]^2 - 4E_t X} \right)}{2E_t}$) due to the tight-binding nature of some of the peptides.

Peptide synthesis. The University of North Carolina (UNC) Peptide Synthesis core facility made the peptides using a modified CarboMAX method and a CEM Liberty Blue microwave synthesizer (51). Fluorescent dyes were coupled manually using acid forms of the dyes and N, N'-di (propan-2-yl) methanediimine (DIPC)/ N, N-diisopropylethylamine (DIEA) in dimethylformamide (DMF).

X-ray crystallography. The crystals were grown at 4°C using the hanging-drop vapor-diffusion method by mixing 1 μ L of purified DDB1 (6 mg/mL) with 1 μ L of reservoir solution that contained 100 mM MES (pH 6.6), 16% PEG 4000, 50 mM NaCl, 5 mM DTT. The Crystals were briefly soaked with 2 μ L of 460 μ M pUL145 H-box peptide and 2 μ L of cryoprotectant (50% ethylene glycol). The data were collected on APS 22ID. Diffraction data were processed using HKL2000, and the structure was solved using molecular replacement in Phenix using DDB1 bound to the H-box of DDB2 (PDB ID 317L), in which the peptide was mutated to the pUL145 sequence. The model was iteratively built and refined using Coot and Phenix, respectively.

Quality score and WebLogos. To generate an alignment of the H-boxes, we took all the crystallized H-box motifs and aligned them based on the 13 positions of the crystallized epitope. We used Jalview to determine the quality score and to color the sequences by conservation (52). We used WebLogo3 as a visual representation of the available residues at each position (53).

Rosetta modeling. To examine residue-residue contacts between DDB1 and various H-box motifs, we used the Rosetta molecular modeling software package (54, 55). First, to prepare the structure for Rosetta, we started with the pUL145-DDB1 complex and removed all the residues between 388 and 711, which correspond to the BPB that binds to CUL4 and is not involved in H-box recognition. The rationale for this deletion is it would speed up the simulations and restrict the number of overall residues that Rosetta would evaluate since the Rosetta score is affected by all atoms in the simulation. We then ran a fast relax with constraints to the native position and took the lowest structure for subsequent modeling steps. Next, we used the fixbb application to mutate the H-box sequence to DCAF1, DDB2, or HBx or to keep the pUL145 sequence. Taking the lowest scoring structure from each of these runs, we ran the relax application again with constraints to the native and generated 100 models for each H-box peptide-DDB1 complex. We took the lowest scoring structure for each complex and used the score_protein_ligand_interactions application to pull out the per-residue score terms. Finally, we summed all the pairwise interaction energies between each residue in the H-box and any residue in DDB1 and plotted those as bar graphs (Fig. 5B to E).

Immunoprecipitation and immunoblot analysis. HEK293T cells were maintained in Dulbecco's minimal essential medium (DMEM) supplemented with 10% fetal bovine serum (FBS), penicillin, streptomycin, and 2 mM glutamine at 37°C in 5% CO₂. HEK293T cells were transfected using polyethylenimine hydrochloride reagent (PEI, Sigma) at a concentration of 3 mg PEI per mg plasmid DNA. To identify the DDB1 and pUL145 mutations that can interrupt the DDB1-pUL145 interaction, HEK293T cells were plated in 100-mm dishes and transfected with FLAG-DDB1 and (3 \times)MYC-UL145 wild-type or mutant plasmids as indicated. Twenty hours after transfection, the cells were washed with ice-cold phosphate-buffered saline (PBS). Subsequently, the cells used for coimmunoprecipitation were lysed by NP-40 lysis buffer (0.5% Nonidet P-40, 50 mM Tris (pH 7.5), 150 mM NaCl, 10% glycerol) containing Halt protease and phosphatase inhibitor (Thermo Scientific), and crude lysates were cleared by centrifugation at 14,000 rpm at 4°C for 15 min. The supernatants were incubated with either anti-FLAG M2 affinity gel (Sigma) for FLAG-IP or homemade MYC3 antibodies coupled to protein A/G-agarose (Thermo Scientific) for MYC-IP. The immunocomplex was washed twice with NP-40 lysis buffer and then three times with PBS. The samples were separated by SDS-PAGE for immunoblot analysis. For STAT2 immunoblots, the total cell lysates were obtained by using radioimmunoprecipitation assay (RIPA) buffer (50 mM Tris (pH 8.0), 0.1% SDS, 150 mM NaCl, 1% Nonidet P-40, 0.5% sodium deoxycholate, and protease inhibitor cocktail). The following antibodies were used for the immunoblot analysis: mouse monoclonal anti-FLAG M2 (Sigma), rabbit polyclonal homemade anti-MYC3, mouse monoclonal anti-STAT2(B-3) (Santa Cruz), and mouse monoclonal anti-glyceraldehyde-3-phosphate dehydrogenase (GAPDH) (GeneTex).

Data availability. The atomic coordinates and structure factors used in this study have been deposited in the RCSB Protein Data Bank (PDB) under accession number 7UKN.

ACKNOWLEDGMENTS

We thank Stuart Endo-Streeter and John Sondek for their help with processing of the X-ray diffraction data. Data were collected at Southeast Regional Collaborative Access Team (SER-CAT) 22-ID Beamline at the Advanced Photon Source, Argonne National Laboratory. The peptides were synthesized by Krzysztof Krajewski at the UNC Peptide Synthesis core facility (RRID:SCR_017837).

SER-CAT is supported by its member institutions, and equipment grants (S10_RR25528, S10_RR028976 and S10_OD027000) from the National Institutes of Health (NIH). Use of the Advanced Photon Source was supported by the U.S. Department of Energy, Office of Science, Office of Basic Energy Sciences, under contract W-31-109-Eng-38. Our work is also supported by NIH grant P30CA016086 (to the UNC Center for Structural Biology); NIH grant R01CA163834 (to A.S.B. and Y.X.); NIH grants R01CA068377, R01AI127346, and

R01GM067113 (to Y.X.); startup funds from university of the pacific (UoP) (to J.S.H.); and the UNC University Cancer Research Fund, and NIH grant R35GM128855 (to N.G.B.).

E.T.W., C.J.T., Z.L., N.I.N., and Z.R. designed research supervised by A.S.B., Y.X., J.S.H., and N.G.B.; E.T.W., C.J.T., Z.L., N.I.N., Z.R., and J.S.H. performed research and/or contributed new reagents; E.T.W., N.I.N., A.S.B., Y.X., J.S.H., and N.G.B. analyzed data; and E.T.W., J.S.H., and N.G.B. wrote the paper.

Y.X. is an inventor named on patent applications filed by UNC. The Xiong laboratory has received research funds from Cullgen, Inc. Y.X. is an equity shareholder in and employee of Cullgen, Inc. The other authors declare no conflict of interest.

REFERENCES

- Chamontin C, Bossis G, Nisole S, Arhel NJ, Maarifi G. 2021. Regulation of viral restriction by post-translational modifications. *Viruses* 13:2197. <https://doi.org/10.3390/v13112197>.
- Rothenburg S, Brennan G. 2020. Species-specific host-virus interactions: implications for viral host range and virulence. *Trends Microbiol* 28:46–56. <https://doi.org/10.1016/j.tim.2019.08.007>.
- Le-Trilling VTK, Trilling M. 2020. Ub to no good: how cytomegaloviruses exploit the ubiquitin proteasome system. *Virus Res* 281:197938. <https://doi.org/10.1016/j.virusres.2020.197938>.
- Curtis NL, Bolanos-Garcia VM. 2019. The anaphase promoting complex/cyclosome (APC/C): a versatile E3 ubiquitin ligase. *Subcell Biochem* 93: 539–623. https://doi.org/10.1007/978-3-030-28151-9_18.
- Rape M. 2018. Ubiquitylation at the crossroads of development and disease. *Nat Rev Mol Cell Biol* 19:59–70. <https://doi.org/10.1038/nrm.2017.83>.
- Ohtake F, Tsuchiya H, Saeki Y, Tanaka K. 2018. K63 ubiquitylation triggers proteasomal degradation by seeding branched ubiquitin chains. *Proc Natl Acad Sci U S A* 115:E1401–E1408. <https://doi.org/10.1073/pnas.1716673115>.
- Yau RG, Doerner K, Castellanos ER, Haakonsen DL, Werner A, Wang N, Yang XW, Martinez-Martin N, Matsumoto ML, Dixit VM, Rape M. 2017. Assembly and function of heterotypic ubiquitin chains in cell-cycle and protein quality control. *Cell* 171:918–933.e20. <https://doi.org/10.1016/j.cell.2017.09.040>.
- Ohtake F, Saeki Y, Ishido S, Kanno J, Tanaka K. 2016. The K48-K63 branched ubiquitin chain regulates NF- κ B signaling. *Mol Cell* 64:251–266. <https://doi.org/10.1016/j.molcel.2016.09.014>.
- Erpapazoglou Z, Walker O, Haguenaer-Tsapis R. 2014. Versatile roles of K63-linked ubiquitin chains in trafficking. *Cells* 3:1027–1088. <https://doi.org/10.3390/cells3041027>.
- Nathan JA, Kim HT, Ting L, Gygi SP, Goldberg AL. 2013. Why do cellular proteins linked to K63-polyubiquitin chains not associate with proteasomes? *EMBO J* 32:552–565. <https://doi.org/10.1038/emboj.2012.354>.
- Haakonsen DL, Rape M. 2019. Branching out: improved signaling by heterotypic ubiquitin chains. *Trends Cell Biol* 29:704–716. <https://doi.org/10.1016/j.tcb.2019.06.003>.
- Proulx J, Borgmann K, Park IW. 2021. Role of virally-encoded deubiquitinating enzymes in regulation of the virus life cycle. *Int J Mol Sci* 22:4438. <https://doi.org/10.3390/ijms22094438>.
- Liu Y, Tan X. 2020. Viral manipulations of the cullin-RING ubiquitin ligases. *Adv Exp Med Biol* 1217:99–110. https://doi.org/10.1007/978-981-15-1025-0_7.
- Sette P, Nagashima K, Piper RC, Bouamr F. 2013. Ubiquitin conjugation to Gag is essential for ESCRT-mediated HIV-1 budding. *Retrovirology* 10:79. <https://doi.org/10.1186/1742-4690-10-79>.
- Jager S, Gottwein E, Krausslich HG. 2007. Ubiquitination of human immunodeficiency virus type 1 Gag is highly dependent on Gag membrane association. *J Virol* 81:9193–9201. <https://doi.org/10.1128/JVI.00044-07>.
- Welker L, Paillart JC, Bernacchi S. 2021. Importance of viral late domains in budding and release of enveloped RNA viruses. *Viruses* 13:1559. <https://doi.org/10.3390/v13081559>.
- Mortensen F, Schneider D, Barbic T, Sladewska-Marquardt A, Kuhnle S, Marx A, Scheffner M. 2015. Role of ubiquitin and the HPV E6 oncoprotein in E6AP-mediated ubiquitination. *Proc Natl Acad Sci U S A* 112:9872–9877. <https://doi.org/10.1073/pnas.1505923112>.
- Baek K, Scott DC, Schulman BA. 2021. NEDD8 and ubiquitin ligation by cullin-RING E3 ligases. *Curr Opin Struct Biol* 67:101–109. <https://doi.org/10.1016/j.sbi.2020.10.007>.
- Greenwood EJD, Williamson JC, Sienkiewicz A, Naamati A, Matheson NJ, Lehner PJ. 2019. Promiscuous targeting of cellular proteins by Vpr drives systems-level proteomic remodeling in HIV-1 infection. *Cell Rep* 27: 1579–1596.e7. <https://doi.org/10.1016/j.celrep.2019.04.025>.
- Murphy CM, Xu Y, Li F, Nio K, Reszka-Blanco N, Li X, Wu Y, Yu Y, Xiong Y, Su L. 2016. Hepatitis B virus X protein promotes degradation of SMC5/6 to enhance HBV replication. *Cell Rep* 16:2846–2854. <https://doi.org/10.1016/j.celrep.2016.08.026>.
- Jackson S, Xiong Y. 2009. CRL4s: the CUL4-RING E3 ubiquitin ligases. *Trends Biochem Sci* 34:562–570. <https://doi.org/10.1016/j.tibs.2009.07.002>.
- Angers S, Li T, Yi X, MacCoss MJ, Moon RT, Zheng N. 2006. Molecular architecture and assembly of the DDB1-CUL4A ubiquitin ligase machinery. *Nature* 443:590–593. <https://doi.org/10.1038/nature05175>.
- He YJ, McCall CM, Hu J, Zeng Y, Xiong Y. 2006. DDB1 functions as a linker to recruit receptor WD40 proteins to CUL4-ROC1 ubiquitin ligases. *Genes Dev* 20:2949–2954. <https://doi.org/10.1101/gad.1483206>.
- Higa LA, Wu M, Ye T, Kobayashi R, Sun H, Zhang H. 2006. CUL4-DDB1 ubiquitin ligase interacts with multiple WD40-repeat proteins and regulates histone methylation. *Nat Cell Biol* 8:1277–1283. <https://doi.org/10.1038/ncb1490>.
- Jin J, Arias EE, Chen J, Harper JW, Walter JC. 2006. A family of diverse Cul4-Ddb1-interacting proteins includes Cdt2, which is required for S phase destruction of the replication factor Cdt1. *Mol Cell* 23:709–721. <https://doi.org/10.1016/j.molcel.2006.08.010>.
- Minor MM, Hollinger FB, McNeese AL, Jung SY, Jain A, Hyser JM, Bissig KD, Slagle BL. 2020. Hepatitis B virus HBx protein mediates the degradation of host restriction factors through the cullin 4 DDB1 E3 ubiquitin ligase complex. *Cells* 9:834. <https://doi.org/10.3390/cells9040834>.
- Lee J, Zhou P. 2007. DCAF1, the missing link of the CUL4-DDB1 ubiquitin ligase. *Mol Cell* 26:775–780. <https://doi.org/10.1016/j.molcel.2007.06.001>.
- Fischer ES, Scrima A, Bohm K, Matsumoto S, Lingaraju GM, Faty M, Yasuda T, Cavadini S, Wakasugi M, Hanaoka F, Iwai S, Gut H, Sugawara K, Thoma NH. 2011. The molecular basis of CRL4DDB2/CSA ubiquitin ligase architecture, targeting, and activation. *Cell* 147:1024–1039. <https://doi.org/10.1016/j.cell.2011.10.035>.
- Scrima A, Konickova R, Czyzewski BK, Kawasaki Y, Jeffrey PD, Groisman R, Nakatani Y, Iwai S, Pavletich NP, Thoma NH. 2008. Structural basis of UV DNA-damage recognition by the DDB1-DDB2 complex. *Cell* 135:1213–1223. <https://doi.org/10.1016/j.cell.2008.10.045>.
- Wu Y, Zhou X, Barnes CO, DeLucia M, Cohen AE, Gronenborn AM, Ahn J, Calero G. 2016. The DDB1-DCAF1-Vpr-UNG2 crystal structure reveals how HIV-1 Vpr steers human UNG2 toward destruction. *Nat Struct Mol Biol* 23: 933–940. <https://doi.org/10.1038/nsmb.3284>.
- Li T, Robert El, van Breugel PC, Strubin M, Zheng N. 2010. A promiscuous α -helical motif anchors viral hijackers and substrate receptors to the CUL4-DDB1 ubiquitin ligase machinery. *Nat Struct Mol Biol* 17:105–111. <https://doi.org/10.1038/nsmb.1719>.
- Li T, Chen X, Garbutt KC, Zhou P, Zheng N. 2006. Structure of DDB1 in complex with a paramyxovirus V protein: viral hijack of a propeller cluster in ubiquitin ligase. *Cell* 124:105–117. <https://doi.org/10.1016/j.cell.2005.10.033>.
- Decorsiere A, Mueller H, van Breugel PC, Abdul F, Gerossier L, Beran RK, Livingston CM, Niu C, Fletcher SP, Hantz O, Strubin M. 2016. Hepatitis B virus X protein identifies the SMC5/6 complex as a host restriction factor. *Nature* 531:386–389. <https://doi.org/10.1038/nature17170>.
- Lin GY, Paterson RG, Richardson CD, Lamb RA. 1998. The V protein of the paramyxovirus SV5 interacts with damage-specific DNA binding protein. *Virology* 249:189–200. <https://doi.org/10.1006/viro.1998.9317>.

35. Le-Trilling VTK, Becker T, Nachshon A, Stern-Ginossar N, Scholer L, Voigt S, Hengel H, Trilling M. 2020. The human cytomegalovirus pUL145 isoforms act as viral DDB1-cullin-associated factors to instruct host protein degradation to impede innate immunity. *Cell Rep* 30:2248–2260.e5. <https://doi.org/10.1016/j.celrep.2020.01.070>.
36. Nightingale K, Lin KM, Ravenhill BJ, Davies C, Nobre L, Fielding CA, Ruckova E, Fletcher-Etherington A, Soday L, Nichols H, Sugrue D, Wang ECY, Moreno P, Umrana Y, Huttlin EL, Antrobus R, Davison AJ, Wilkinson GWG, Stanton RJ, Tomasec P, Weekes MP. 2018. High-definition analysis of host protein stability during human cytomegalovirus infection reveals antiviral factors and viral evasion mechanisms. *Cell Host Microbe* 24:447–460.e11. <https://doi.org/10.1016/j.chom.2018.07.011>.
37. Karlin D, Belshaw R. 2012. Detecting remote sequence homology in disordered proteins: discovery of conserved motifs in the N-termini of Mononegavirales phosphoproteins. *PLoS One* 7:e31719. <https://doi.org/10.1371/journal.pone.0031719>.
38. Darby JF, Hopkins AP, Shimizu S, Roberts SM, Brannigan JA, Turkenburg JP, Thomas GH, Hubbard RE, Fischer M. 2019. Water networks can determine the affinity of ligand binding to proteins. *J Am Chem Soc* 141:15818–15826. <https://doi.org/10.1021/jacs.9b06275>.
39. Precious B, Childs K, Fitzpatrick-Swallow V, Goodbourn S, Randall RE. 2005. Simian virus 5 V protein acts as an adaptor, linking DDB1 to STAT2, to facilitate the ubiquitination of STAT1. *J Virol* 79:13434–13441. <https://doi.org/10.1128/JVI.79.21.13434-13441.2005>.
40. Nightingale K, Potts M, Hunter LM, Fielding CA, Zerbe CM, Fletcher-Etherington A, Nobre L, Wang ECY, Strang BL, Houghton JW, Antrobus R, Suarez NM, Nichols J, Davison AJ, Stanton RJ, Weekes MP. 2022. Human cytomegalovirus protein RL1 degrades the antiviral factor SLFN11 via recruitment of the CRL4 E3 ubiquitin ligase complex. *Proc Natl Acad Sci U S A* 119:e2108173119. <https://doi.org/10.1073/pnas.2108173119>.
41. Salsman J, Jagannathan M, Paladino P, Chan PK, Dellaire G, Raught B, Frappier L. 2012. Proteomic profiling of the human cytomegalovirus UL35 gene products reveals a role for UL35 in the DNA repair response. *J Virol* 86:806–820. <https://doi.org/10.1128/JVI.05442-11>.
42. Mahon C, Krogan NJ, Craik CS, Pick E. 2014. Cullin E3 ligases and their rewiring by viral factors. *Biomolecules* 4:897–930. <https://doi.org/10.3390/biom4040897>.
43. Becker T, Le-Trilling VTK, Trilling M. 2019. Cellular cullin RING ubiquitin ligases: druggable host dependency factors of cytomegaloviruses. *Int J Mol Sci* 20:1636. <https://doi.org/10.3390/ijms20071636>.
44. Benhenda S, Ducroux A, Riviere L, Sobhian B, Ward MD, Dion S, Hantz O, Protzer U, Michel ML, Benkirane M, Semmes OJ, Buendia MA, Neuveut C. 2013. Methyltransferase PRMT1 is a binding partner of HBx and a negative regulator of hepatitis B virus transcription. *J Virol* 87:4360–4371. <https://doi.org/10.1128/JVI.02574-12>.
45. Tsuge M, Hiraga N, Akiyama R, Tanaka S, Matsushita M, Mitsui F, Abe H, Kitamura S, Hatakeyama T, Kimura T, Miki D, Mori N, Imamura M, Takahashi S, Hayes CN, Chayama K. 2010. HBx protein is indispensable for development of viraemia in human hepatocyte chimeric mice. *J Gen Virol* 91:1854–1864. <https://doi.org/10.1099/vir.0.019224-0>.
46. Keasler VV, Hodgson AJ, Madden CR, Slagle BL. 2007. Enhancement of hepatitis B virus replication by the regulatory X protein *in vitro* and *in vivo*. *J Virol* 81:2656–2662. <https://doi.org/10.1128/JVI.02020-06>.
47. Reichermeier KM, Straube R, Reitsma JM, Sweredoski MJ, Rose CM, Moradian A, den Besten W, Hinkle T, Verschueren E, Petzold G, Thoma NH, Wertz IE, Deshaies RJ, Kirkpatrick DS. 2020. PIKES analysis reveals response to degraders and key regulatory mechanisms of the CRL4 network. *Mol Cell* 77:1092–1106.e9. <https://doi.org/10.1016/j.molcel.2019.12.013>.
48. Lv L, Wang Q, Xu Y, Tsao LC, Nakagawa T, Guo H, Su L, Xiong Y. 2018. Vpr targets TET2 for degradation by CRL4(VprBP) E3 ligase to sustain IL-6 expression and enhance HIV-1 replication. *Mol Cell* 70:961–970.e5. <https://doi.org/10.1016/j.molcel.2018.05.007>.
49. Nobre LV, Nightingale K, Ravenhill BJ, Antrobus R, Soday L, Nichols J, Davies JA, Seirafian S, Wang EC, Davison AJ, Wilkinson GW, Stanton RJ, Huttlin EL, Weekes MP. 2019. Human cytomegalovirus interactome analysis identifies degradation hubs, domain associations and viral protein functions. *Elife* 8:e49894. <https://doi.org/10.7554/eLife.49894>.
50. Hilgarth RS, Lanigan TM. 2020. Optimization of overlap extension PCR for efficient transgene construction. *MethodsX* 7:100759. <https://doi.org/10.1016/j.mex.2019.12.001>.
51. Collins JM, Porter KA, Singh SK, Vanier GS. 2014. High-efficiency solid phase peptide synthesis (HE-SPPS). *Org Lett* 16:940–943. <https://doi.org/10.1021/ol4036825>.
52. Waterhouse AM, Procter JB, Martin DM, Clamp M, Barton GJ. 2009. Jalview version 2—a multiple sequence alignment editor and analysis workbench. *Bioinformatics* 25:1189–1191. <https://doi.org/10.1093/bioinformatics/btp033>.
53. Crooks GE, Hon G, Chandonia JM, Brenner SE. 2004. WebLogo: a sequence logo generator. *Genome Res* 14:1188–1190. <https://doi.org/10.1101/gr.849004>.
54. Koehler Leman J, Weitzner BD, Renfrew PD, Lewis SM, Moretti R, Watkins AM, Mulligan VK, Lyskov S, Adolf-Bryfogle J, Labonte JW, Kryz J, RosettaCommons C, Bystruff C, Schief W, Gront D, Schueler-Furman O, Baker D, Bradley P, Dunbrack R, Kortemme T, Leaver-Fay A, Strauss CEM, Meiler J, Kuhlman B, Gray JJ, Bonneau R, RosettaCommons Consortium. 2020. Better together: elements of successful scientific software development in a distributed collaborative community. *PLoS Comput Biol* 16:e1007507. <https://doi.org/10.1371/journal.pcbi.1007507>.
55. Leman JK, Weitzner BD, Lewis SM, Adolf-Bryfogle J, Alam N, Alford RF, Aprahamian M, Baker D, Barlow KA, Barth P, Basanta B, Bender BJ, Blacklock K, Bonet J, Boyken SE, Bradley P, Bystruff C, Conway P, Cooper S, Correia BE, Coventry B, Das R, De Jong RM, DiMaio F, Dsilva L, Dunbrack R, Ford AS, Frenz B, Fu DY, Geniesse C, Goldschmidt L, Gowthaman R, Gray JJ, Gront D, Guffy S, Horowitz S, Huang PS, Huber T, Jacobs TM, Jeliakov JR, Johnson DK, Kappel K, Karanicolos J, Khakzad H, Khar KR, Khare SD, Khatib F, Khrumushin A, King IC, Kleffner R, et al. 2020. Macromolecular modeling and design in Rosetta: recent methods and frameworks. *Nat Methods* 17:665–680. <https://doi.org/10.1038/s41592-020-0848-2>.